American Mineralogist, Volume 82, pages 781–789, 1997

Experimental investigation of laumontite → wairakite + H_2O: A model diagenetic reaction

CARLOS JOVÉ* AND BRADLEY R. HACKER†

Department of Geological and Environmental Sciences, Stanford University, Stanford, California 94305, U.S.A.

ABSTRACT

The rate and mechanism of a key diagenetic reaction, laumontite → wairakite + H_2O, have been determined in experiments with durations as long as three months at P_{H_2O} = 100 MPa and temperatures of 350–450 °C. In the lower temperature range, 350–400 °C, nucleation of wairakite occurred on the smallest laumontite fragments in the starting material. Growth then proceeded by the dissolution of large laumontite grains, transport within the fluid, and precipitation of euhedral to subhedral wairakite. At higher temperatures, 425 and 450 °C, each sample contains two product phases: wairakite and an unidentified plagioclase-like phase. The plagioclase-like silicate was stabilized by the uptake of Na and formed early as ~10 μm wide skeletal grains along laumontite grain boundaries. The wairakite grains subsequently nucleated on and grew into the interiors of large laumontite grains.

Nucleation rates at 425–450 °C were 10–100 wairakite grains per square meter of laumontite surface per second. Growth rates varied from 1.5×10^{-11} m/s at 350 °C to 2.1×10^{-10} m/s at 450 °C; the low-temperature data can be fit with an apparent activation energy of 72 ± 13 kJ/mol and a pre-exponential "interface jump distance" of $\sim 1 \times 10^{-18}$ m. This activation energy and these growth rates are comparable to those calculated by Walther and Wood (1984) to characterize interface-controlled reactions in silicates under H_2O-saturated conditions. Our data predict transformation rates for geologic conditions that are too fast to account for the commonly observed incomplete natural reaction of laumontite → wairakite, indicating that transformation in nature must be limited by slower nucleation rates or by slower intergranular diffusion—perhaps as a result of lower H_2O activity or slower heating rates.

INTRODUCTION

The role of fluid in the Earth's crust is multifaceted and profound. The presence and activity of fluid influence rock deformation, heat flow, the distribution of stable isotopes, the maturation of hydrocarbons, the formation of hydrothermal ore deposits, the earthquake failure process, magma formation, and the state of stress in the crust (Nur and Walder 1990). Processes of enormous economic consequence within the upper crust—hazardous seismicity and the formation, migration, entrapment, and degradation of hydrocarbons—are influenced by devolatilization reactions during diagenesis. However, few kinetic studies have been conducted on materials actively undergoing low-grade metamorphism or diagenesis. Therefore our understanding of the rates at which devolatilization occurs and of the effects devolatilization has on porosity, permeability, and deformation is limited. This paper focuses on a single devolatilization reaction that is active during diagenesis: laumontite → wairakite + H_2O. Laumontite is a common low-grade metamorphic zeolite, with equilibrium phase relations and thermodynamic properties that are reasonably well understood. Besides being an important mineral in its own right, laumontite breakdown also serves as a model system for polyphase rocks. We report on the rate and mechanism of laumontite breakdown during hydrostatic experiments.

LAUMONTITE AND HYDROCARBONS

Laumontite, $CaAl_2Si_4O_{12} \cdot 4H_2O$, is the diagnostic mineral of the zeolite facies (Cho et al. 1986; Liou et al. 1987). It is a widespread, low-grade alteration product of calcic plagioclase, volcanic glass, lithic fragments, calcareous fossils, and other zeolites; it also occurs as precipitates in veins (Boles and Coombs 1977; Helmold and van de Kamp 1984). In oil fields, laumontite most commonly forms within plagioclase crystals and often contains inclusions of sericite and epidote formed during plagioclase breakdown. Laumontite cements develop in feldspathic sandstones and can comprise up to 20 vol% of rocks in petroleum fields (e.g., the Stevens sandstone

* Present address: Laboratoire de Geochimie, Universite Paul Sabatier, 38 rue des Trente Six Ponts, Toulouse, France

† Present address: Geology Department, University of California, Santa Barbara, California 93106-9630, U.S.A.

0003–004X/97/0708–0781$05.00

in the San Joaquin, Boles 1984; Tertiary sandstones in the Santa Ynez Mountains, Helmold and van de Kamp 1984; and eastern Georgia, Soviet Union, Vernik 1990). Laumontite cement has a drastic effect on porosity, leading to reductions of 5–20 percentage points (Galloway 1979; Surdam and Boles 1979). Well-developed laumontite occludes all porosity (Helmold and van de Kamp 1984), destroying reservoirs and forming seals to fluid movement. Laumontite may also play a salient role in crustal fault zones as it is present as fracture fillings in cataclastic zones within several active fault zones (Evans and Chester 1995; James and Silver 1988; Surdam and Boles 1979; Vernik and Nur 1992).

Laumontite crystallization occurs at depths of 1–3 km at temperatures as low as 50–65 °C (Boles and Coombs 1977; Galloway 1979; Helmold and van de Kamp 1984) and usually postdates all other diagenetic activity except late calcite cementation (Helmold and van de Kamp 1984). It is widely accepted that the appearance of laumontite cement in a drill hole heralds economic basement, because of the typical pervasiveness of laumontite cement and its relative insolubility in carbonic acid. However, laumontite eventually breaks down to other calcium aluminum silicates such as wairakite at greater depths in response to increased temperature or pressure or decreased a_{H_2O}. This disappearance of laumontite produces secondary porosity either because of replacement by minerals with smaller molar volumes or hydrofracturing associated with the release of H_2O structurally bound in the laumontite (Vernik 1990).

Laumontite transforms to wairakite ($CaAl_2Si_4O_{12}{\cdot}2H_2O$) + H_2O at temperatures in excess of ~300 °C, and it transforms to lawsonite + quartz + H_2O at pressures above ~300 MPa (Liou 1971; Fig. 1). Liou's early experiments on the equilibrium phase relations of laumontite and related minerals provide preliminary information about the rate at which laumontite decomposes to form other phases. For example, laumontite is stable to temperatures of 346 °C at 200 MPa for periods of up to 1000 h, whereas at only 30 °C higher, laumontite decomposes in less than 150 h (Liou 1971).

Experimental methodology

Natural vein laumontite collected from the Himalaya Mine in San Diego, California by W. Kleck of Pure-Minerals, was ground in an agate mortar and sieved dry to 100–300 μm. The mineral powder was washed repeatedly in an ultrasonic bath for 20–30 minute intervals to disaggregate fine particles, resieved, purified using methylene iodide and magnetic separation, and then repeatedly washed in an ultrasonic bath of distilled water. Savage et al. (1993) demonstrated that 10% HCl and acetone produced "considerable grain size reduction and pronounced surface etching" of laumontite, so we avoided such treatment. The purity of the starting material was verified by X-ray diffraction (XRD), electron-probe microanalalysis (EPMA), and optical microscopy. XRD showed no phases other than laumontite, optical microscopy revealed ≪1% calcite, and EPMA showed ~1% of an unidentified acicular phase of the composition $Ca_4Al_{0.7}Si_{4.5}O_{12}{\cdot}H_2O$ (Table 1).

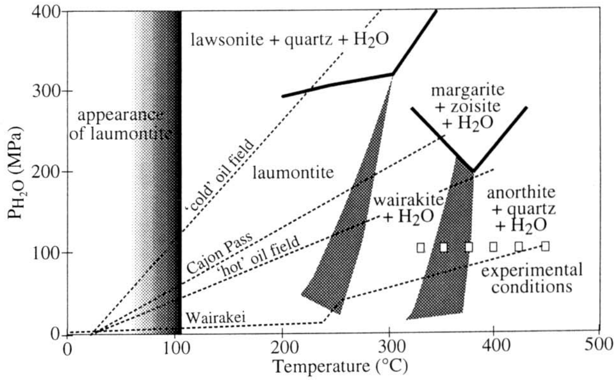

Figure 1. Equilibrium stability fields for minerals in the system CaO-Al_2O_3-SiO_2-$2H_2O$. Ranges of conditions shown for the laumontite → wairakite and wairakite → anorthite + quartz reactions are based on Berman (1988) and Johnson et al. (1992); the experimental stabilities determined by Liou (1971) lie within these ranges. Lawsonite and margarite stabilities calculated using the thermodynamic database of Berman (1988). Laumontite appears in rocks at temperatures of 50 °C and persists stably to ~230 °C at 100 MPa in oil fields, the Cajon Pass drillhole on the San Andreas Fault (Lachenbruch and Sass 1992), and the Wairakei geothermal area (Steiner 1977). Experimental conditions for the present kinetic study are shown by squares.

The experiments were conducted in vertically mounted, externally heated cold-seal pressure vessels (Kerrick 1987) using water as the pressure medium. P_{H_2O} was fixed at 100 MPa, and temperatures of 350, 375, 400, 425, and 450 °C were maintained for periods of up to three months (Fig. 1). Each isothermal set of experiments was conducted in a single apparatus to eliminate differences in apparatus behavior. Temperature and confining pressure uncertainty are ±5 °C and ±5 MPa. By moving a second thermocouple up and down inside the vessel we determined that the maximum temperature difference over the length of the experimental capsule was 1 °C.

Then 100 mg of laumontite and 12–15 μL of double-distilled water were loaded into 2.2 mm diameter and 20 mm long gold capsules. The solid material filled about 70% of each capsule; the other half of the capsule was flattened before welding. The H_2O evolved during the experiments inflated the capsule as necessary to maintain inside the capsule the same pressure as that outside the capsule. The initial porosity of these grain aggregates was 15–20 vol%, as determined by backscattered electron (BSE) imaging. The loaded capsules were weighed before and after each experiment to check for leaks. When a capsule was found to have leaked, the experiment was repeated. However, no textural or kinetic differences were noted between sealed and unsealed capsules, presumably because the fluid composition and pressure were similar inside and outside the capsules.

TABLE 1. Wavelength-dispersive electron-microprobe analyses

	Laumontite, $n = 3$	Wairakite, $n = 3$	Acicular phase, $n = 2$	Plagioclase(?), $n = 4$
SiO_2	51.12 ± 0.43	55.44 ± 0.46	58.63 ± 0.50	55.31 ± 0.81
Al_2O_3	22.61 ± 0.19	23.66 ± 0.39	7.77 ± 0.11	28.17 ± 0.49
CaO	12.33 ± 0.10	12.42 ± 0.15	24.12 ± 0.33	13.87 ± 0.40
Na_2O				1.28 ± 0.21
K_2O				0.15 ± 0.04
Sum	86.07 ± 0.63	91.45 ± 0.31	90.53 ± 0.94	98.78 ± 0.68
	O = 12, H = 4	O = 12, H = 2	O = 12, H = 2	O = 8, H = 0
Si	3.95 ± 0.01	4.01 ± 0.01	4.49 ± 0.01	2.51 ± 0.03
Al	2.06 ± 0.01	2.01 ± 0.01	0.70 ± 0.01	1.50 ± 0.03
Ca	1.02 ± 0.01	0.96 ± 0.01	3.95 ± 0.01	0.67 ± 0.02
Na				0.11 ± 0.02
K				0.01 ± 0.00

Notes: Operating conditions on JEOL 733: 15 kV operating voltage, 15 nA sample current, and 10 μm spotsize. Ti, Fe, Cr, Mn, and Mg were analyzed but are below detection limits for all phases; no other elements were identified by energy-dispersive spectrometry. Na and K were below detection for three of the four phases. Each analysis was computed with a ZAF correction using the O and H anions shown.

The primary means of sample characterization were optical microscopy, scanning electron microscopy, and electron-probe microanalysis of doubly polished thin sections. The thin sections were prepared by impregnating a capsule with epoxy and sawing it in half, thus preserving the transformation texture. The extent of transformation was determined by capturing backscattered electron images digitally and analyzing them using NIH Image software; replicate analyses of different portions of the same samples revealed an uncertainty of 1–2 percentage points.

Grain sizes were also determined using computer analysis of digital BSE images. The uncertainty in the measurement of an individual grain diameter is ~0.5 μm. The grain size of laumontite in untransformed samples is chiefly 150–200 μm, but a wide size range of smaller grains was produced during capsule loading and pressurization; the laumontite is so fragile that this is unavoidable. Laumontite grains in untransformed samples exhibit weak undulatory extinction and cracks largely along cleavage planes. Wairakite growth rates were computed by measuring the grain sizes in each section. Minimum nucleation rates were computed by counting the average number n of individual wairakite grains attached to single laumontite grains, dividing by the duration of the experiment t, and correcting for sectioning effects:

$$\dot{n} = (n/2\pi Rzt)\,(2rz/\pi r^2) \qquad (1)$$

where R is the radius of a laumontite grain, πRz is the surface area of that grain contained within a section of thickness z, πr^2 is the area of the interface between a laumontite grain and a single wairakite grain of radius r, and $2rz$ is the area of such an interface contained within a section.

Liou (1971) used X-ray diffraction to determine that some of his synthetically produced wairakite was in the disordered tetragonal form. However, other experimental studies on the hydrothermal synthesis of wairakite (Ames and Sand 1958; Koizumi and Roy 1960; Wirsching 1981) did not find disorder using X-ray diffraction. We examined some of our samples by X-ray diffraction, but did not detect disordered wairakite; no phases other than wairakite and laumontite were observed by X-ray diffraction either. However, a small fraction, ~1%, of the laumontite grains in the starting material contain bladed hydrous calcium aluminosilicate crystals that we presume are a zeolite ("acicular phase" in Table 1).

OBSERVATIONS

Experiments conducted between 350 and 450 °C for periods of 40–1517 h produced extents of transformation varying from 1–99% (Table 2; Fig. 2). There are clear textural differences between the samples heated at low (350–400 °C) and high (425 and 450 °C) temperatures. At small degrees of transformation, each low-temperature sample contains widely spaced wairakite grains. The wairakite grains appear in the optical microscope to have a subuniform grain size, but quantitative image analysis revealed a range of grain sizes (Fig. 3). These low-temperature wairakite grains generally grew as distinct grains and did not replace or grow directly into laumontite crystals (Fig. 4A). They typically are euhedral where they project into voids and are anhedral where impinging on laumontite crystals. Most of these wairakite grains have translucent rims developed on dusty-looking cores; the cores contain high densities of fluid inclusions (up to 5 vol%) visible with scanning electron microscopy. At higher degrees of transformation, the wairakite grains formed at 350–400 °C impinge on one another and are physically separated from the laumontite crystals that are breaking down (Fig. 4B).

Each weakly transformed high-temperature (425 and 450 °C) sample contains two product phases: wairakite and a plagioclase-like mineral. The plagioclase-like silicate occurs as ~10 μm thick skeletal grains along laumontite-laumontite grain boundaries (Fig. 4C). Electron-probe analyses (Table 2) show measurable Na and K, neither of which was recognized in the starting material. Oxide totals are ~99% and no unanalyzed elements were recognized by wavelength-dispersive spectrometry that could account for the mass deficit; we presume therefore that the mineral contains ~1 wt% H_2O. The compositions are charge balanced and can be represented as mixtures

TABLE 2. Experimental results

No.	t (hr)	d_{avg} (μm)	d_{max} (μm)	ξ	ξ_{min}	ξ_{max}	'plg'	$\dot{n}$
		350 °C, ΔG = −10.4 kJ/mol						
3	196	24.7 ± 3.1	30	0.01	0.01	0.04	0	
6	360	31.4 ± 4.4	37	0.02	0.01	0.03	0	
7	744	72.3 ± 7.6	85	0.05	0.02	0.08	0	
14	1517	116 ± 8.8	128	0.43	0.43	1.00	0	
		375 °C, ΔG = −13.8 kJ/mol						
19	70	33.6 ± 5.9	46	0.02	0.02	0.05	0	
22	134	31.2 ± 4.3	39	0.03	0.02	0.03	0	
21	134	32.9 ± 3.5	37	0.03	0.01	0.03	0	
1	210	37.0 ± 4.0	43	0.39	0.38	0.40	0	
17	240	46.3 ± 7.7	55	0.03	0.02	0.07	0	
24	428	67.4 ± 9.0	83	0.13	0.10	0.20	0	
9	470	89.8 ± 14.3	113	0.29	0.27	0.29	0	
10	755	139 ± 20.5	175	0.37	0.30	0.43	0	
30	1137	142 ± 19.6	182	0.45	0.28	0.46	0	
15	1515	303 ± 30.9	346	0.99	0.99	1.00	0	
		400 °C, ΔG = −17.2 kJ/mol						
16	50	23.5 ± 3.5	31	0.03	0.03	0.04	0	
20	56	32.0 ± 4.1	39	0.05	0.02	0.06	0	
8	101	31.6 ± 4.4	40	0.02	0.02	0.03	0	
12	101	52.8 ± 5.2	62	0.13	0.12	0.17	0	
13	115	59.6 ± 7.0	71	0.35	0.18	0.41	0	
29	128	65.8 ± 9.4	81	0.82	0.71	0.90	0	
2	194	64.9 ± 9.0	81	0.50	0.49	0.54	0	
18	240	88.0 ± 7.5	100	0.63	0.61	0.72	0	
4	407	113 ± 13.7	132	0.72	0.44	0.86	0	
23	457	158 ± 22.8	201	0.32	0.20	0.33	0	
		425 °C, ΔG = −20.7 kJ/mol						
27	74	34.2 ± 7.8	58	0.07	0.05	0.09	0.02	99
48	103	32.3 ± 5.9	43	0.05	0.03	0.05	0.00	82
49	129	38.8 ± 5.6	52	0.08	0.05	0.09	0.00	59
38	168	67.4 ± 13.1	96.4	0.78	0.76	0.79	0.05	n.d.
26	169	56.2 ± 7.7	71	0.26	0.16	0.27	0.01	50
11	232	56.3 ± 6.1	75				0.02	n.d.
37	264	90.9 ± 11.1	110	0.78	0.55	0.78	0.06	16
25	380	121 ± 9.6	133	0.92	0.89	0.92	0.08	n.d.
		450 °C, ΔG = −24.3 kJ/mol						
60	40	30.1 ± 9.3	55	0.01	0.00	0.01	0.02	54
55	45	56.6 ± 8.5	71	0.01	0.00	0.01	0.04	22
58	49	33.9 ± 9.2	62	0.08	0.08	0.11	0.08	220
57	80	51.1 ± 13.0	87	0.06	0.02	0.06	0.02	66
56	94	64.9 ± 16.2	103	0.22	0.12	0.22	0.07	61
54	120	107 ± 29.8	181	0.02	0.01	0.02	0.03	27
62	144	102 ± 34.5	194	0.37	0.15	0.46	0.07	n.d.
61	168	109 ± 30.9	184	0.07	0.04	0.21	0.09	n.d.

Notes: t: duration of experiments; d_{avg}: mean and standard deviation of grain size; d_{max}: maximum grain size; ξ: mean fraction of wairakite; ξ_{min}: minimum fraction of wairakite; ξ_{max}: maximum fraction of wairakite; plg: fraction of plagioclase(?); $\dot{n}$: nucleation rate.

of albite + anorthite + wairakite + analcite. The abundance of this plagioclase-like phase ranges from 0–6 vol% (average 4 vol%) at 425 °C to 1–9 vol% (average 5 vol%) at 450 °C; it is unrelated to experiment duration and depends weakly on temperature (Table 2). The wairakite grains formed at 425 and 450 °C are anhedral and grew into laumontite crystals—a morphology quite different from the low temperature samples. At higher degrees of transformation, the wairakite grains impinged on one another and eventually grew together to produce a rock of modest porosity. Dissolution features, such as tunnels, are weakly developed in laumontite at 425 °C and strongly developed at 450 °C (Fig. 4D).

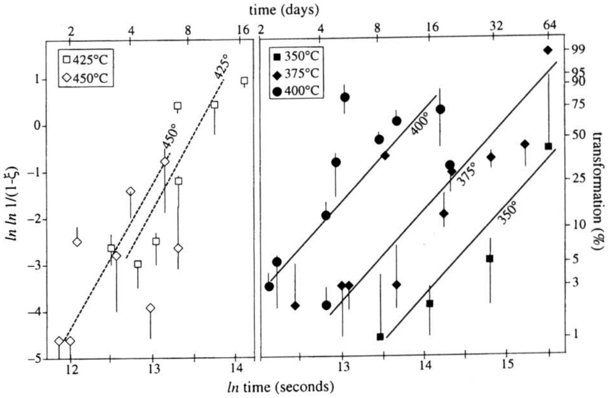

FIGURE 2. Temperature and time dependence of the transformation of laumontite to wairakite at 100 MPa. Each datum represents the mean extent of transformation, and the vertical bars are the range of transformation observed within a single sample. Transformation (%) and time (days) axes are logarithmic.

Reaction mechanisms

The distribution of grain sizes in the low-temperature (350–400 °C) samples (Fig. 3) indicates that nucleation occurred early in the experiments and was subsequently slow relative to the growth rate of existing nuclei; if the nucleation rate had been constant throughout the experiments, the grain sizes should comprise a seriate range, including micrometer-scale grains. That wairakite grains fill void space and are not attached to laumontite grains suggests that nucleation took place on micrometer-scale laumontite grains in the starting material and not on the surfaces of the large laumontite grains. The discrete separation between wairakite and laumontite also indicates that reaction occurred by the dissolution of laumontite, transport within the fluid, and precipitation of wairakite. Although no textural evidence of laumontite dissolution was observed in the low-temperature (<400 °C) samples, the lack of contact between laumontite and wairakite and the euhedral nature of the wairakite grains support this interpretation. The absence of dissolution features suggests that wairakite growth, and not laumontite breakdown, was the rate-limiting process (Berner 1981).

The distribution of wairakite grain sizes in the high-temperature (425 and 450 °C) samples also indicates that nucleation occurred early in the experiments and was subsequently slow relative to the growth rate. That the majority of wairakite grains are contained within large laumontite grains and only infrequently project into voids or form isolated grains suggests that: (1) wairakite was forced to nucleate on the large laumontite grains because the plagioclase-like phase consumed all the high-energy micrometer-scale laumontite grains; and (2) growth occurred by direct (topotaxial?) replacement of laumontite by wairakite, instead of by dissolution, long-range transport, and precipitation. Laumontite grains that lack wairakite but exhibit dissolution features must have contrib-

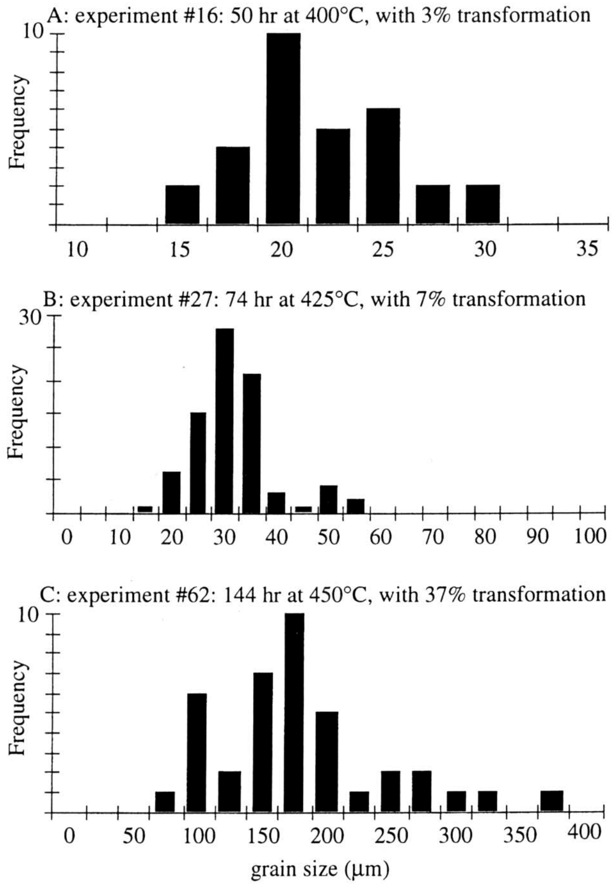

FIGURE 3. Histograms of wairakite grain sizes for three samples.

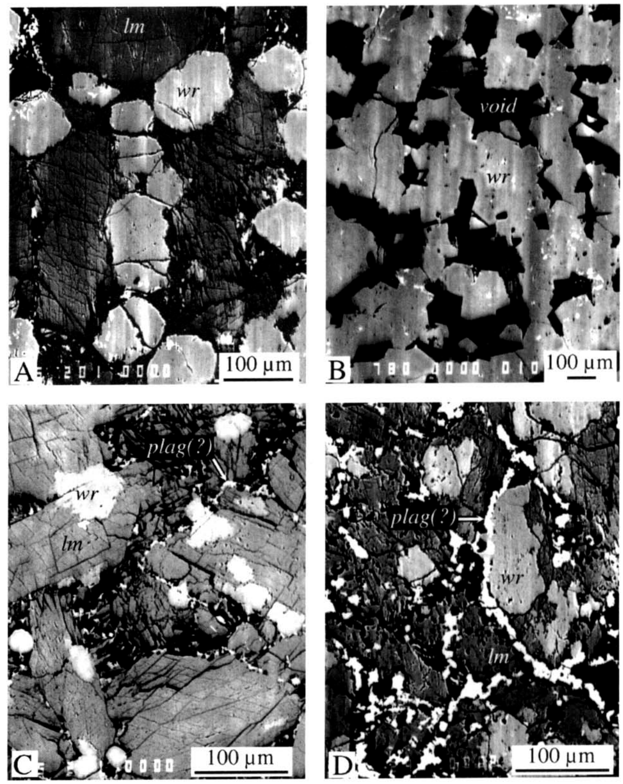

FIGURE 4. Textures formed by the breakdown of laumontite to wairakite + H_2O. (**A**) Low degrees of transformation at 350–400 °C consists of widely spaced wairakite grains grown on small fragments suspended in the fluid. (**B**) High degrees of transformation at 350–400 °C consists of wairakite grains that have grown together. (**C**) Low degrees of transformation at 425–450 °C consists of minor plagioclase(?) grown along laumontite grain boundaries and wairakite growing within laumontite grains. (**D**) High degrees of transformation at 425–450 °C are characterized by large wairakite grains and strong dissolution features in the laumontite.

uted material to distant, growing wairakite grains by means of diffusion through the fluid.

Reaction rates

Johnson and Mehl's original formulation of an equation to describe transformation as a function of nucleation and growth rate was modified by Avrami (1939, 1940, 1941) to allow for early site saturation and by Cahn (1956) to account more specifically for early saturation of nucleation sites on grain corners, edges, and surfaces. All are of the form

$$\xi = 1 - \exp(-K \dot{x}^m t^n) \tag{2}$$

where ξ is the amount of transformation, K, m, and n are constants, $\dot{x}$ is growth rate, and t is time. As emphasized by Rubie and Thompson (1985), meaningful application of these equations or their more general time-derivative form (Cahn 1957) to experimental data requires a careful assessment of grain size, nucleation rate, growth rate, and growth morphology. Most kinetic studies have avoided measurement of nucleation rate and growth rate, and many have also eschewed textural observations, attempting instead to fit values of K, m, and n to the above equation empirically. In these empirical approaches the value of m or n has typically been used to make inferences about the geometry of growth or the sites of nucleation rather than using reaction textures to evaluate growth and nucleation. Assessment of a reaction mechanism should come from textural observations and not from the empirical values of m or n (Rubie and Thompson 1985).

The textures described above indicate that the reaction mechanism in our samples was essentially instantaneous nucleation followed by interface-controlled growth. Turnbull's (1956) formulation to quantify growth rate, $\dot{x}$, during interface-controlled reactions is:

$$\dot{x} = \frac{\delta k T}{h} e^{-Q/RT}[1 - e^{-\Delta G/RT}] \tag{3}$$

where δ is an interface jump distance, k is Boltzmann's constant, T is absolute temperature, h is Planck's constant, Q is the apparent activation energy, and R is the universal gas constant. This formulation, unlike the Johnson-Mehl–

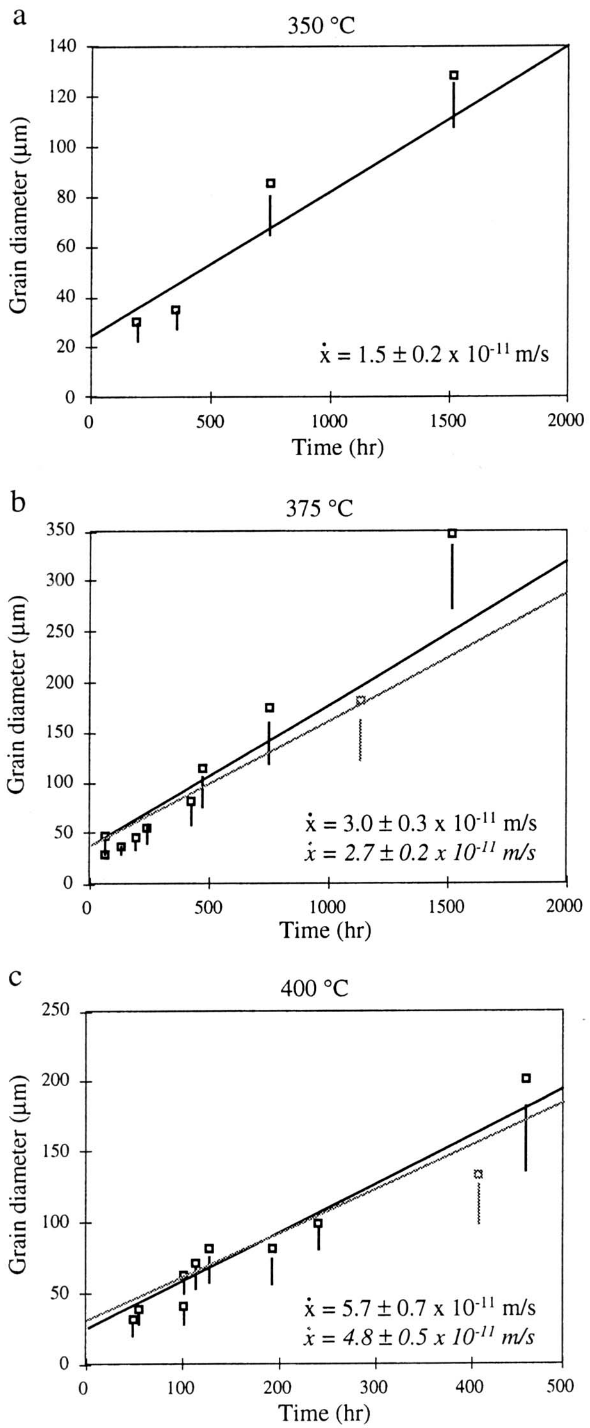

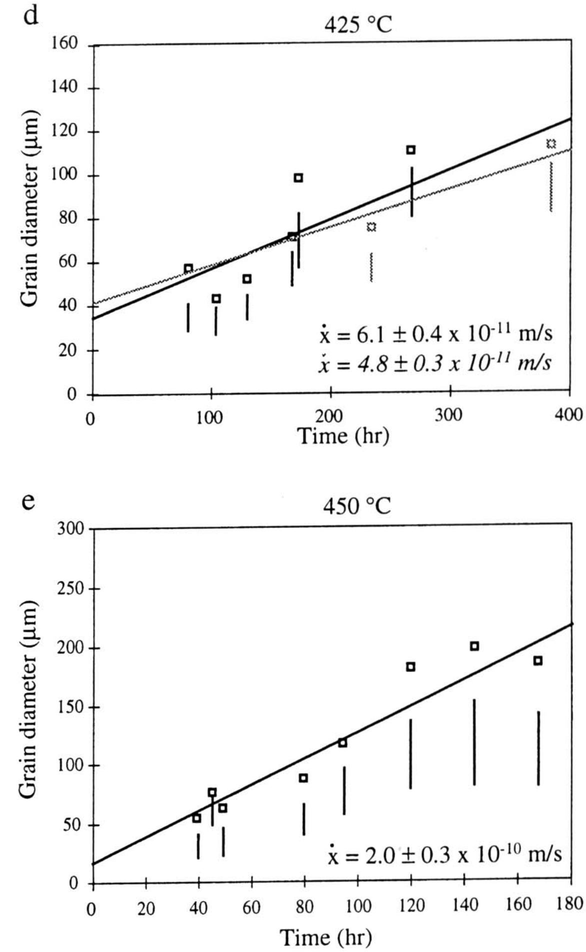

FIGURE 5. Wairakite grain growth. Squares indicate maximum grain diameters, and bars show one standard deviation about the mean grain diameters. Grain growth was calculated as the change in maximum grain diameter per unit time; Monte-Carlo fits to all the black-colored data are shown in black, and fits including the grayed data are shown in gray.

Avrami equation, includes the Gibbs free energy of the reaction, ΔG. We calculated this free energy for each experiment using the program SUPCRT92 (Johnson et al. 1992).

Nucleation in the high-temperature (425 and 450 °C) samples occurred on laumontite surfaces. By counting the number of wairakite grains per unit area of a BSE image and normalizing to the laumontite surface area sampled by the image, we calculate nucleation rates of 10–100 wairakite grains per square meter of laumontite surface per second. Nucleation in the low-temperature (350–400 °C) samples cannot be quantified because nucleation occurred on micrometer-scale laumontite fragments no longer visible.

Growth rates were determined by measuring grain size as a function of experiment duration (Fig. 5). Each panel of Figure 5 shows the size of the largest grain measured, as well as the distribution of grain sizes defined by one standard deviation about the mean grain size. Each of the data sets defines a linear trend that defines the growth rate. Some have distinctly non-zero intercepts, indicating literally a finite grain size at time zero. We suggest that the early stages of growth were extremely rapid and gave way within relatively short time to constant, slower growth rate. The rapid reaction was probably due to the presence of surface defects because we chose not to etch the starting material. Savage et al. (1993) also observed an early, more rapid phase of laumontite dissolution that they attributed to the consumption of very fine-grained reactants present in the starting material. We propose that the linear portion of the data more accurately characterizes the reaction of undamaged mineral surfaces (Holdren and Berner 1979).

Growth rates were quantified at each experimental temperature by fitting measured maximum grain diameters vs. experiment duration. Thus, the maximum grain diameter accurately reflected the end result of growth and not delayed nucleation followed by growth, which could be the process that created smaller grains. The uncertainty of each maximum grain size datum was assumed to have a Gaussian distribution equal to the standard deviation of the mean grain size. The fitting procedure was a Monte-Carlo method that randomly chose 10 000 grain sizes for each experiment duration and calculated a least-squares minimization. As expected, the growth rate increases with temperature from 1.5×10^{-11} m/s at 350 °C to 2.1×10^{-10} m/s at 450 °C. Between 400 and 425 °C, however, there is a discontinuity in growth rate concomitant with the change in reaction mechanism discussed earlier. Note that had we chosen to calculate growth rates using average rather than maximum grain diameters, the growth rates would be ~33% slower, but the calculated activation energies (see below) would be the same.

The apparent activation energies for grain growth were also fit by means of a Monte-Carlo method assuming Gaussian uncertainties for the growth rates. Our textural observations suggest different reaction mechanisms for the 350–400 °C and the 425–450 °C experiments, and the data of Figure 6 highlight a matching discontinuity in growth rates. If these two data sets are fitted independently, they yield apparent activation energies of $Q_l = 72 \pm 13$ kJ/mol and $Q_h = 196 \pm 27$ kJ/mol (Fig. 6). Fits to the three low-temperature data plus the 425 °C or the 450 °C growth rates give $Q_3 = 62.4 \pm 8.1$ kJ/mol and $Q_4 = 89.5 \pm 7.1$ kJ/mol, respectively. Neither of these latter fits should have physical significance because of the inferred change in reaction mechanism and are given here only for completeness. For activation energies of 72 ± 13 kJ/mol and 196 ± 27 kJ/mol, the Turnbull equation yields interface jump distances, δ, of $\sim 1 \times 10^{-18}$ m and $\sim 2 \times 10^{-9}$ m. The latter number is close to zeolite lattice spacings of $\sim 10^{-9}$ m, but the former is much smaller, suggesting that either the Turnbull formalism is not an appropriate way of describing the growth kinetics, or that the pre-exponential interface jump distance term of the Turnbull equation cannot be equated with lattice spacing. Hacker et al. (1992) obtained a similarly small δ for growth of aragonite from calcite.

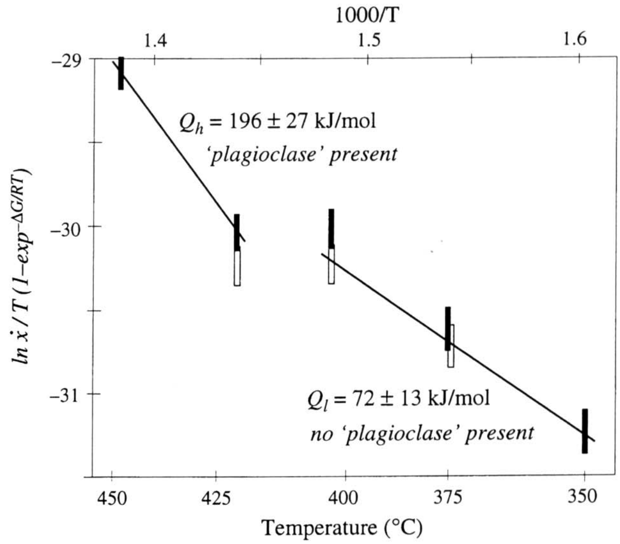

FIGURE 6. Apparent activation energies for the growth of wairakite from laumontite at 100 MPa and 350–450 °C fit to a logarithmic form of Turnbull's growth rate equation: $[\dot{x}/T(1 - e^{-\Delta G/RT})] = \ln(\delta k/h) - Q/RT$. Unfilled and filled data correspond to gray and black fits in Figure 5.

DISCUSSION

Kinetic analysis

Walther and Wood (1984) argued that at small degrees of overstepping, numerous reactions involving the dissolution of relatively insoluble hydrous or anhydrous phases within an H_2O-rich fluid display a consistent relationship between reaction rate dm/dt, temperature T, and reaction free energy ΔG:

$$\frac{\mathrm{d}m}{\mathrm{d}t} = -K\frac{\Delta G}{RT} = -10^{-(2900/T-6.85)}\frac{\Delta G}{RT}. \tag{4}$$

If the rate constant K, is written as an Arrhenius equation:

$$K = Ae^{-Q/RT} \tag{5}$$

the pre-exponential constant A is $10^{6.85}$, and the apparent activation energy is:

$$Q = \ln(10) \times 2900 \times 8.314 \text{ J/mol} = 55.5 \text{ kJ/mol}. \tag{6}$$

In other words, Walther and Wood suggested that reactions controlled by interfacial attachment and detachment of atoms diffused through an H_2O-rich fluid have activation energies in the neighborhood of 55 kJ/mol. Their prediction does not apply to transformations involving diffusion through a solid nor to reactions on highly soluble minerals limited by fluid transport (Berner 1981). Savage et al. (1993) calculated an equivalent activation energy of ~58 kJ/mol for the incongruent dissolution of laumontite into undersaturated H_2O of pH 7–10. The ac-

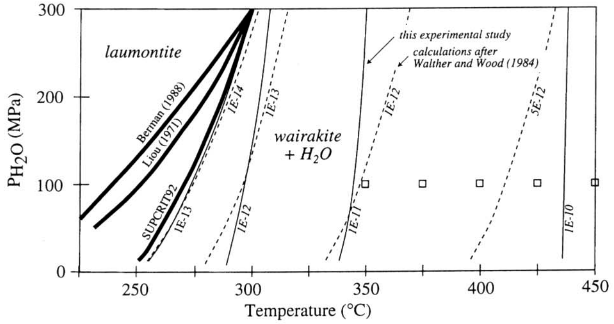

FIGURE 7. Extrapolated growth rate contours (m/s) for wairakite over a range of pressures and temperatures. Solid lines are from experiments reported in this paper; dotted lines correspond to the predictions of Walther and Wood (1984). The slopes of the lines derive from the pressure dependence of the Gibbs free energy of reaction. Squares show experimental conditions. Three possible equilibrium boundaries for the reaction are shown, but the growth-rate contours apply specifically to the SUPCRT92 curve calculated after Johnson et al. (1992).

tivation energy we have measured for wairakite growth of 72 ± 13 kJ/mol is probably equivalent to that of Walther and Wood (1984) and Savage et al.(1993), although neither of the earlier papers explicitly calculated an uncertainty.

Extrapolation of our experimental data to calculate the rate of laumontite growth in geologic situations is straightforward as long as one assumes that the reaction in nature is also interface controlled. To extrapolate the overall transformation rate is more problematic because we measured only a minimum nucleation rate and cannot define its dependence on strain free energy, interfacial free energy, Gibbs free energy, temperature, and other factors. Thus, one must assume a nucleation rate to calculate a transformation rate in nature. Note also that our experiments were conducted at conditions where $a_{H_2O} = 1$. Under natural conditions where $a_{H_2O} < 1$, the reduction in Gibbs free energy can be calculated, but the reaction mechanism and rate may change.

Our experimentally determined growth rates were extrapolated to lower temperatures and pressures of ≤ 300 MPa in Figure 7, using an activation energy of 72 kJ/mol and a value of 1.4×10^{-18} m for δ in Equation 2. Even for Gibbs free energies of reaction less than 1 kJ/mol and temperatures as low as 250 °C, the growth rate is 1×10^{-14} m/s, fast enough to yield 100 μm grains in 10^{10} s or 320 years. The incomplete transformation of laumontite to wairakite observed in rocks indicates that growth in nature is slower than this. Thus, the growth rate under H_2O-saturated conditions must not be the rate-limiting step in the transformation. Some other step during the transformation of laumontite to wairakite must be slower. Candidates include the nucleation rate, intergranular diffusion rate, or heating rate. The effects of a reduction in the activity of H_2O cannot be evaluated quantitatively. The Gibbs free energy of reaction is enhanced by a reduction in a_{H_2O}, which would drive the reaction more rapidly, but the nucleation rate or growth rate could be significantly slower. Equally possible is that a reduction in a_{H_2O} will mean that the transport of species within the intergranular fluid may drop dramatically and become the rate-limiting step. Under such conditions it is even possible that laumontite may dissolve and the solute be advected from the reaction site faster than wairakite can grow. Walther and Wood's (1984) equation predicts growth rates about ten times slower than we observed in our experiments (Fig. 7).

Absence of anorthite

Experiments conducted at temperatures ≥ 400 °C—and possibly ≥ 350 °C, depending on the applicability of experiments by Liou (1971) or calculations based on Berman (1988) or Johnson et al. (1992)—were in the stability field of anorthite + quartz. In spite of this, we did not find quartz or anorthite in any of our experimental samples. The plagioclase-like phase we observed at 425 and 450 °C may be analogous to the formation of pure anorthite, but its growth was likely controlled by the availability of Na and K, and, in any case, its growth period was limited and followed by much more extensive growth of wairakite. This is noteworthy because the wairakite formed outside its stability field at temperatures as high as 450 °C, where the Gibbs free energy of the reaction wairakite → anorthite + quartz + H_2O is −3 to −5 kJ/mol.

ACKNOWLEDGMENTS

Acknowledgment is made to the Department of Energy and the Donors of The Petroleum Research Fund, administered by the American Chemical Society, for the support of this research. Helpful reviews were given by J.W. Carey and W.-L. Huang.

REFERENCES CITED

Ames, L.L. and Sand, L.B. (1958) Hydrothermal synthesis of wairakite and calcium-mordenite. American Mineralogist, 43, 476–480.
Avrami, M. (1939) Kinetics of phase change, I: general theory, Journal of Chemical Physics, 7, 1103–1112.
———(1940) Kinetics of phase change, II: Transformation-time relations for random distribution of nuclei, Journal of Chemical Physics, 8, 212–224.
———(1941) Kinetics of phase change, III: granulation, phase change, and microstructure, Journal of Chemical Physics, 9, 177–184.
Berman, R.G. (1988) Internally-consistent thermodnamic data for minerals in the system Na_2O-K_2O-CaO-MgO-FeO-Fe_2O_3-Al_2O_3-SiO_2-TiO_2-H_2O-CO_2. Journal of Petrology, 29, 445–522.
Berner, R.A. (1981) Kinetics of weathering and diagenesis. Kinetics of geochemical processes. In Mineralogical Society of America Reviews in Mineralogy, 8, 111–132.
Boles, J.R. (1984) Secondary porosity reactions in the Stevens Sandstone, San Joaquin Valley, California. American Association of Petroleum Geologists Memoir, 37, 217–224.
Boles, J.R. and Coombs, D.S. (1977) Zeolite-facies alteration of sandstones in the Southland syncline, New Zealand. American Journal of Science, 277, 982–1012.
Cahn, J.W. (1956) The kinetics of grain boundary nucleated reactions. Acta Metallurgica, 4, 449–459.
———(1957) On the kinetics of the pearlite reaction. American Institute of Mining and Metallurgical Engineers Transactions, 209, 140–145.
Cho, M., Liou, J.G., and Maruyama, S. (1986) Transition from the zeolite

to prehnite-pumpellyite facies in the Karmutsen metabasits, Vancouver Island, British Columbia. Journal of Petrology, 27, 467–494.

Evans, J.P. and Chester, F.M. (1995) Fluid-rock interaction in faults of the San Andreas system; inferences from San Gabriel Fault rock geochemistry and microstructures. Journal of Geophysical Research, 100, 13,007–13,020.

Galloway, W.E. (1979) Diagenetic control of reservoir quality in arc-derived sandstones: implications for petroleum exploration. In P.A. Scholle and P.R. Schluger, Eds., Aspects of Diagenesis: Society of Economic Paleontologists and Mineralogists Special Publications, 26, p. 251–261. Society of Economic Paleontologists and Mineralogists, Tulsa, OK.

Hacker, B.R., Kirby, S.H., and Bohlen, S.R. (1992) Time and metamorphic petrology: the calcite → aragonite transformation. Science, 258, 110–113.

Helgeson, H.C., Delaney, J.M., Nesbitt, H.W., and Bird, D.K. (1978) Summary and critique of the thermodynamic properties of rock-forming minerals. American Journal of Science, 278–A 229 pp.

Helmold, K.P. and van de Kamp, P.C. (1984) Diagenetic mineralogy and controls on albitization and laumontite formation in Paleogene arkoses, Santa Ynez Mountains, California. American Association of Petroleum Geologists Memoir, 37, 239–276.

Holdren, G.R. and Berner, R.A. (1979) Mechanism of feldspar weathering, I, experimental studies. Geochimica Cosmochimica et Acta, 43, 1161–1171.

James, E.W. and Silver, L.T. (1988) Implications of zeolites and their zonation in the Cajon Pass deep drillhole. Geophysical Research Letters, 15, 973–976.

Johnson, J.W., Oelkers, E.H., and Helgeson, H.C. (1992) SUPCRT92: A software package for calculating the standard molal thermodynamic properties of mineral, gases, aqueous species, and reactions from 1 to 5000 bars and 0 to 1000 °C. Computers and Geosciences, 18, 899–947.

Kerrick, D.M. (1987) Cold-seal systems. In G.C. Ulmer, and H.L. Barnes, Eds., Hydrothermal experimental techniques, p. 293–323. Wiley, New York.

Koizumi, M. and Roy, R. (1960) Zeolite studies. I. Synthesis and stability of the calcium zeolites. Journal of Geology, 68, 41–53.

Lachenbruch, A.L. and Sass, J.H. (1992) Heat flow from Cajon Pass, fault strength, and tectonic implications. Journal of Geophysical Research, 97, 4995–5015.

Liou, J.G. (1971) P-T stabilities of laumontite, wairakite, lawsonite, and related minerals in the system $CaAl_2Si_2O_8$-SiO_2-H_2O. Journal of Petrology, 12, 379–411.

Liou, J.G., Maruyama, S., and Cho, M. (1987) Very low-grade metamorphism of volcanic and volcaniclastic rocks—mineral assemblages and mineral facies. In M. Frey, Ed., Low Temperature Metamorphism, p. 59–112. Blackie, Glasgow.

Nur, A. and Walder, J. (1990) Time-dependent hydraulics of the Earth's crust. In The Role of Fluids in Crustal Processes, p. 113–127. National Academy Press, Washington, D.C..

Rubie, D.C. and Thompson, A.B. (1985) Kinetics of metamorphic reactions at elevated temperatures and pressures: an appraisal of available experimental data. In A.B. Thompson and D.C. Rubie, Eds., Metamorphic Reactions; Kinetics, Textures, and Deformation, Advances in Physical Geochemistry, 4, p. 27–79. Springer-Verlag, New York.

Savage, D., Cave, M.R., Haigh, D., Milodowski, A.E., and Young, M.E. (1993) The reaction kinetics of laumontite under hydrothermal conditions. European Journal of Mineralogy, 5, 523–535.

Steiner, A. (1977) The Wairakei geothermal area North Island, New Zealand. New Zealand Geological Survey Bulletin, 90, 136.

Surdam, R.C. and Boles, J.R. (1979) Diagenesis of volcanic sandstones. In Scholle, P.A. and Schluger, P.R., Eds., Aspects of Diagenesis, 26, p. 227–242. Society of Economic Paleontologists and Mineralogists Special Publication, Tulsa, OK.

Turnbull, D. (1956) Phase changes. Solid State Physics, 3, 225–306.

Vernik, L. (1990) A new type of reservoir rock in volcaniclastic sequences. American Association of Petroleum Geologists Bulletin, 74, 830–836.

Vernik, L. and Nur, A. (1992) Petrophysical analysis of the Cajon Pass Scientific Well: implications for fluid flow and seismic studies in the continental crust. Journal of Geophysical Research, 97, 5121–5134.

Walther, J.V. and Wood, B.J. (1984) Rate and mechanism in prograde metamorphism. Contributions to Mineralogy and Petrology, 88, 246–259.

Wirsching, U. (1981) Experiments on the hydrothermal formation of calcium zeolites. Clays and Clay Minerals, 29, 171–183.

MANUSCRIPT RECEIVED AUGUST 5, 1996
MANUSCRIPT ACCEPTED MARCH 10, 1997